

# Relation of substorm disturbances triggered by abrupt solar-wind changes to physics of plasma sheet transport

L. R. Lyons, D.-Y. Lee, C.-P. Wang, and S. B. Mende

**Abstract:** Substorm onset occurs within the near-Earth plasma sheet in the region that maps to the Harang electric field reversal observed within the ionosphere. IMF changes that are expected to reduce the convection electric field after  $\gtrsim 25$  min of negative IMF  $B_z$  are well known to cause substorms. Solar wind dynamic pressure  $P_{dyn}$  enhancements following prolonged strongly southward IMF ( $B_z \lesssim -8$  nT) also cause substorms. However, an interplay of effects from a simultaneous IMF and  $P_{dyn}$  change can prevent the occurrence of a substorm, leading to what we refer to as null events. We show that the combination of inward convection and energy-dependent magnetic drift in the finite-width plasma sheet offers an explanation for the IMF and pressure triggered substorms, for their onset within the Harang reversal region, and for the null events. These same aspects of the plasma sheet transport also offer an explanation for the growth-phase development of the Harang reversal, for steady-magnetospheric convection events, and for pseudo-substorms.

*Key words:* Substorms, Harang discontinuity, Dynamic pressure, Plasma sheet.

## 1. Introduction

Abrupt changes in the interplanetary magnetic field (IMF) and solar wind lead to large-scale disturbances of the magnetosphere-ionosphere system and in particular to substorms. Furthermore, auroral observations have been used to show that substorm onset occurs within a region of converging electric fields known as the Harang discontinuity [1, 6, 8, 18, 19, Weygand et al., presented at this conference, 2006]. Note that the Harang discontinuity is a region where the north-south component of electric fields reverses direction, and is not actually a discontinuity. For this reason, it is referred to here as the “Harang reversal.” Observations of ionospheric flows have shown that the Harang reversal enhances during the substorm growth phase and decreases dramatically at onset, implying that the evolution of the Harang reversal is “related to the cause of substorm expansion onsets” [3, Bristow, presented at this conference, 2006].

Here we first describe how disturbance features depend on the type of interplanetary change and identify which changes lead to substorms and which do not. We then describe our proposal for how basic plasma sheet transport leads to the growth phase development of the Harang reversal, causes substorm onset within the Harang reversal, explains why some changes cause substorm onset and others do not, and offers a feasible explanation for steady magnetospheric convection intervals (SMCs, also known as convection bays) and pseudo-substorms (also known as pseudo-breakups).

## 2. Disturbance Features

It is well known that IMF changes that lead to a convection reduction after a  $\gtrsim 25$  min period of negative  $B_z$  lead to the onset of substorms. Global auroral images from the Wideband Imaging Camera (WIC) on board the IMAGE spacecraft are shown in the top row of Fig. 1 for a substorm triggered by an IMF northward turning following a  $\sim 30$  min period of IMF  $B_z \sim -2$  to  $-4$  nT on 9 December 2000 (color images and other data for this and other events discussed here are shown in [16]). These images illustrate what typically is observed for substorms triggered by an IMF change under constant solar wind dynamic pressure,  $P_{dyn}$ .

The images show that brightening within the equatorward portion of the oval was first visible at 1914 UT at  $\sim 00$  to 01 MLT. Such brightening indicates the onset of a substorm expansion. Based on the previous studies referred to in the introduction, this brightening occurs within the region of the Harang reversal. The region of enhanced expansion-phase aurora then spreads azimuthally and poleward over the next 4–6 min, forming a typical aurora bulge and reaching a maximum azimuthal coverage of  $\sim 5$  hr of MLT. This expansion-phase bulge indicates that current-wedge formation occurred within the inner plasma sheet. Consistent with this, the geosynchronous energetic particle data for this event show the clear dispersionless flux enhancements near midnight that result from current wedge formation.

WIC images from 26 July 2000 illustrating the typical auroral response to an increase in  $P_{dyn}$  under steady IMF are shown in the second row of Fig. 1. An enhancement of auroral emissions is observed over a wide range of MLT, both on the dayside and nightside. This enhancement is first clearly seen in the 1857:09 UT image and was as close to simultaneous with the  $P_{dyn}$  impact as can be determined with the 2-min time resolution of WIC. Also note that, unlike for substorms, there is no evidence for bulge formation. Such a global auroral enhancement, without the bulge formation associated with current wedge formation, is the response to the  $P_{dyn}$  driven

Received 15 May 2005.

**L. R. Lyons and C.-P. Wang.** Department of Atmospheric and Oceanic Sciences, University of California, Los Angeles, California, USA.

**D.-Y. Lee.** Department of Astronomy and Space Science, College of Natural Sciences and Institute for Basic Science Research, Chungbuk National University, Chungbuk, South Korea.

**S. B. Mende.** Space Sciences Laboratory, University of California, Berkeley, California, USA.

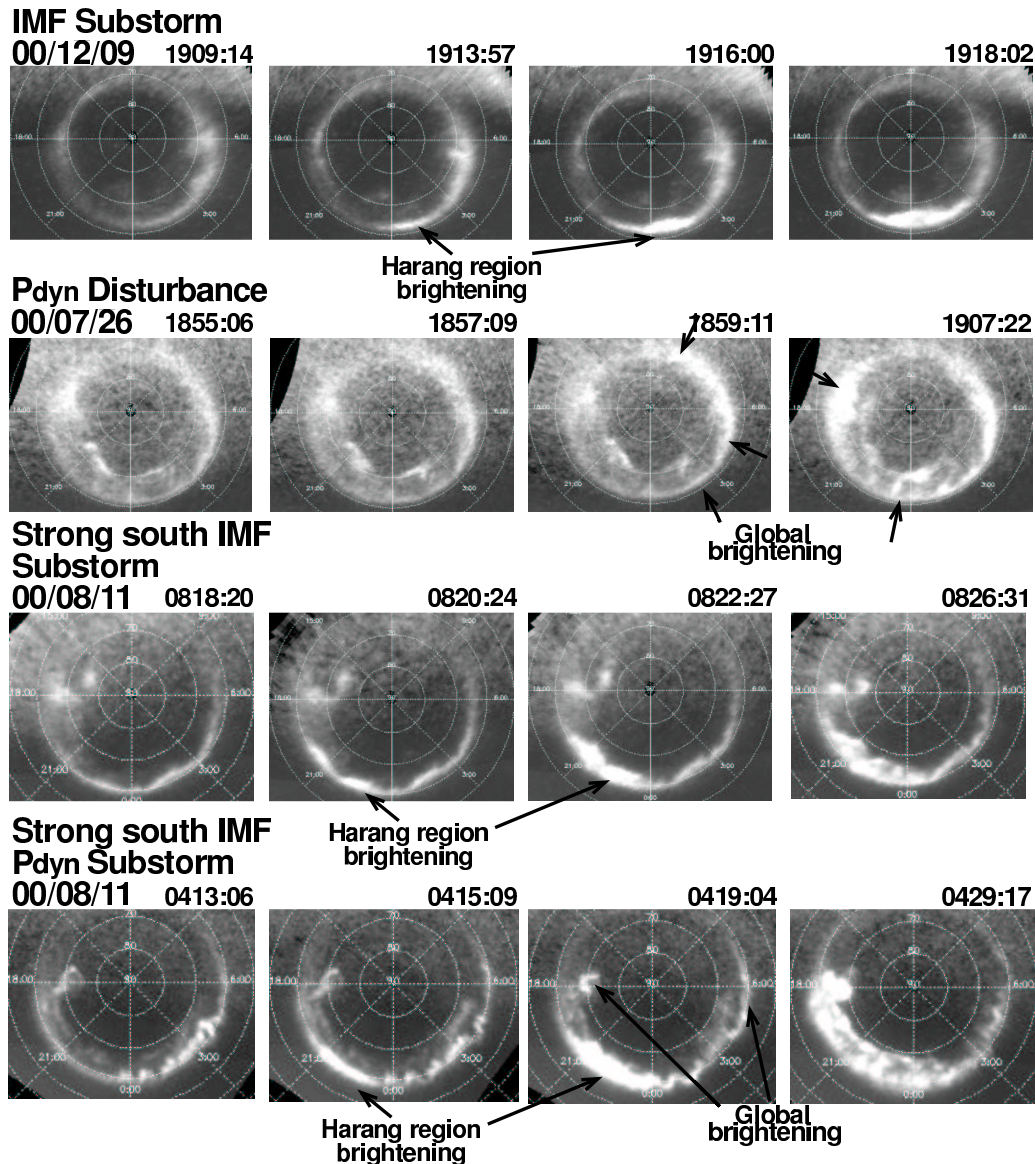


**Fig. 1.** Selected global auroral images from WIC for four different types of events as identified.

compressional heating of plasma sheet electrons, which undergo strong pitch-angle scattering losses to the atmosphere. Direct evidence for a lack of current wedge formation during this type of event has also been found using geosynchronous observations [10]. We attribute most of the global auroral enhancement to enhancement of the diffuse aurora, though some discrete auroral features will also be enhanced due to the increase in the global field-aligned current system that has been observed in response to an increase in  $P_{dyn}$ .

We next address several disturbances that occurred during the 00–12 UT period on 11 August 2000 when the IMF was generally strongly southward at about  $-10$  nT. This period illustrates two important surprises [16]. The IMF and solar wind dynamic pressure for this period from two spacecraft are shown in Fig. 2 as mapped to just in front of the bow shock using the [23] mapping technique.

WIC images for an IMF triggered substorm that followed

$\sim 40$  min of IMF  $B_z \sim -10$  nT are shown in the third row of Fig. 1. This is the second of the two events labeled  $S_{B_z}$  in Fig. 2. The auroral brightening within the expected region of the Harang reversal is first evident in the 0820:24 UT image. The only significant difference from the images for typical substorms is that the region of enhanced expansion-phase aurora after onset spreads azimuthally to a maximum azimuthal coverage of  $\sim 6$ –7 hr of MLT, which is somewhat broader than for the typical substorms. A similar IMF substorm, also labeled  $S_{B_z}$  in Fig. 2, occurred at  $\sim 0640$  UT.

WIC images for a disturbance triggered by an enhancement in  $P_{dyn}$  are shown in the bottom row of Fig. 1, which illustrate the first of our major surprises. Dayside imaging was not particularly good for this event because of sunlight and limitations in the algorithm for subtracting dayglow from the images. However, some auroral brightening can be seen just to the dayside of the dawn-dusk meridian in the 0415:09 and 0419:04 UT

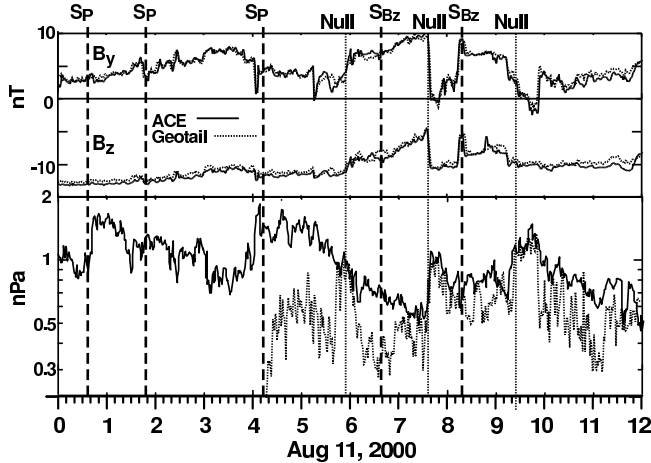


**Fig. 2.** [23]-mapped IMF  $B_y$ ,  $B_z$  and  $P_{dyn}$  from ACE and Geotail, and for 0–12 UT on 11 August 2000. Vertical dashed lines identify events discussed in the text.

images. This is as expected from the magnetospheric compression caused by the pressure enhancement. However, simultaneously, there is a Harang region auroral brightening, which is initially seen at 21–23 MLT in the 0415:09 UT image and then expands azimuthally. The Harang region brightening looks essentially the same as the auroral bulge for northward turning substorms. This suggests that the pressure enhancement led to formation of a substorm current wedge as well as to magnetospheric compression.

The WIC observations thus show evidence for both compressive and substorm auroral enhancements for this  $P_{dyn}$  increase event which occurred following prolonged strongly southward IMF. Furthermore, as the bulge-region aurora expands azimuthally, it seems to merge with the compressive auroral enhancement, particularly on the dusk side. This leads to an unusually broad region of enhanced auroral emissions covering 10–14 hrs of MLT by 0421:17 to 0425:22 UT. Also, clear evidence for current wedge formation within the nightside near-Earth plasma sheet, and for its occurring together with global magnetospheric compression, is seen in the geosynchronous particle data for this event [10]. This event is identified as *SP* in Fig. 2, and there were two other similar events during the time interval shown that are identified in Fig. 2 and were considered along with other such events by [16].

The above events were all selected because they are quite ideal in that there was either an IMF northward turning with approximately steady  $P_{dyn}$  or an increase in  $P_{dyn}$  with approximately steady IMF  $B_z$ . However, it is far more common for a solar wind change to simultaneously affect both  $B_z$  and  $P_{dyn}$ . If increases in solar wind dynamic pressure and northward turnings of the IMF can cause nightside substorm disturbances, it makes sense that effects of changes in these quantities should interact if both occur simultaneously. For example, it would seem that an IMF northward turning accompanied by an increase in  $P_{dyn}$  might lead to a stronger disturbance than would an equal change in only one of the quantities. This idea has not yet been evaluated.

However, the second significant surprise is that we have been able to determine that there indeed is important interaction between effects of IMF  $B_z$  changes and  $P_{dyn}$  changes under

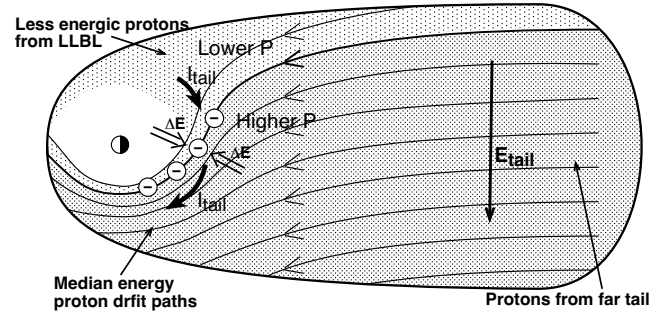


**Fig. 3.** Illustration in the equatorial plane of physics of formation of the Harang reversal. Shaded regions identify the location of the plasma sheet. (based on [5]).

strongly southward IMF conditions when  $P_{dyn}$  decreases (increases) with a simultaneous northward (further southward) turning of the IMF.

Three such events occurred on 11 August 2000 and are identified in Fig. 2 as “Null”. The first had an IMF northward turning from  $B_z < -10$  nT and a simultaneous decrease in  $P_{dyn}$ . The other two events had a further southward IMF turning and an increase in  $P_{dyn}$ . The impacts of the  $P_{dyn}$  changes for these events were clearly seen in the low-latitude H observations. Based on the results from other events, we would expect that the IMF northward turning for the first event and the  $P_{dyn}$  increases for the second two events would, by themselves, have caused a significant, large-scale auroral disturbance. However, the WIC images for these events (see [16]) clearly show that such a disturbance did not occur for these events.

These results for the 11 August 2000 events suggest that the effects of a decrease (increase) in  $P_{dyn}$  and a simultaneous northward (further southward) turning of the IMF can nullify each other, so that a large-scale disturbance, and in particular a substorm response, does not occur.

### 3. Harang Reversal Physics

In order to understand how particle transport associated with the Harang reversal offers an explanation for the types of interplanetary changes discussed above that do, and do not, trigger substorms, it is necessary to first consider the formation of the Harang reversal during the substorm growth phase. This is illustrated in Fig. 3 and can be understood in terms of the equatorial continuity equation for flux tubes

$$\begin{aligned} \frac{\partial}{\partial t}(n\mathcal{V}) + (\mathbf{V}_E \cdot \nabla)(n\mathcal{V}) &= -\frac{\hat{\mathbf{B}}_e \cdot \nabla P \times \nabla \mathcal{V}}{qB_e} \\ &= -\frac{2}{qB_i} j_{\parallel,i} \end{aligned} \quad (1)$$

Here  $\mathbf{V}_E$  is the electric drift velocity,  $n$  is the plasma density,  $\mathcal{V}$  is flux tube volume,  $q$  is the electronic charge,  $j_{\parallel,i}$  is the upward field-aligned current density mapped to the ionosphere, and  $B_e$  and  $B_i$  are the equatorial and ionospheric field strength, respectively. The top portion of (1) is a re-written form of the plasma sheet continuity equation obtained by [7] by integrating the single species mass conservation equation over the volume of a flux tube.

The second term on the left-hand-side of (1) represents a source term to the inner plasma sheet due to inward convection. This leads to an increase in inner plasmasheet flux tube particle content  $n\mathcal{V}$  and plasma pressure after an increase in convection speed. However, as protons drift earthward, the increasing magnetic drift deflects them toward the dusk side as illustrated in Fig. 3. Thus the highest plasma pressure occurs on the dusk side of the inner plasma sheet. Because of the finite width of the tail, higher energy protons from the distant tail do not have access to the dawn side plasma sheet, where such particles must originate from the dawn side low-latitude boundary layer (LLBL). The LLBL source for high-energy protons is far smaller than is the source from the deep tail, and protons reaching the dawn side have moved a smaller distance across the tail, and thus gain less energy from the cross tail electric field than do the particles that reach the dusk side. As a result, pressure at the same radial distance on the dawn side will be less than on the dusk side, giving a significant dawn-to-dusk gradient in pressure within the inner plasma sheet.

Since the magnetic drift speed is proportional to pressure, this azimuthal pressure gradient gives a divergence of proton flux, which is also a divergence of cross tail current. This must be balanced by upward field-aligned current from the ionosphere as given by the well-known relation between  $\nabla P \times \nabla \mathcal{V}$  and  $j_{\parallel,i}$  in (1). However, current continuity must also be maintained in the ionosphere. This requires the formation of electric fields  $\Delta \mathbf{E}$  in the ionosphere that give Pedersen currents that converge towards the region of upward field-aligned currents. These converging electric fields add to the convection electric field to give the reversal of the north-south electric fields that forms the Harang reversal. They also map along field lines to the equatorial plasma sheet as indicated by the  $\Delta \mathbf{E}$  vectors in Fig. 3.

Equation (1) thus allows us to view the local change in  $n\mathcal{V}$  as a balance between a source due to earthward convection, given by  $\mathbf{V}_E \cdot \nabla(n\mathcal{V})$ , and a loss due to divergence driven by magnetic drift. This balance provides a framework for understanding the evolution of the plasma sheet during the substorm growth phase and near the onset of the substorm expansion phase as described by [15]. During periods of weak convection, plasma pressure and  $n\mathcal{V}$  are low throughout the inner plasma sheet and both the source and loss terms in (1) are low. An increase in the strength of convection will increase the particle source due to earthward convection, leading to the increase in plasma pressure and  $n\mathcal{V}$  that gives rise to the substorm growth phase. This will slowly increase the loss term in (1) and simultaneously lead to the growth-phase intensification of the Harang reversal. This increase will continue until either a steady state is reached between sources and losses or the convection strength is reduced so that the source term becomes smaller than the loss term.

#### 4. Steady Magnetospheric Convection Events

Note that a balance between source and loss terms can be reached and allows for a stable plasma sheet configuration without substorms during periods of enhanced convection [21, 22], as occurs during steady magnetospheric convection events (SMCs). This occurs without the pressure inconsistency of [4] because the loss term in (1) is the same divergence that gives a

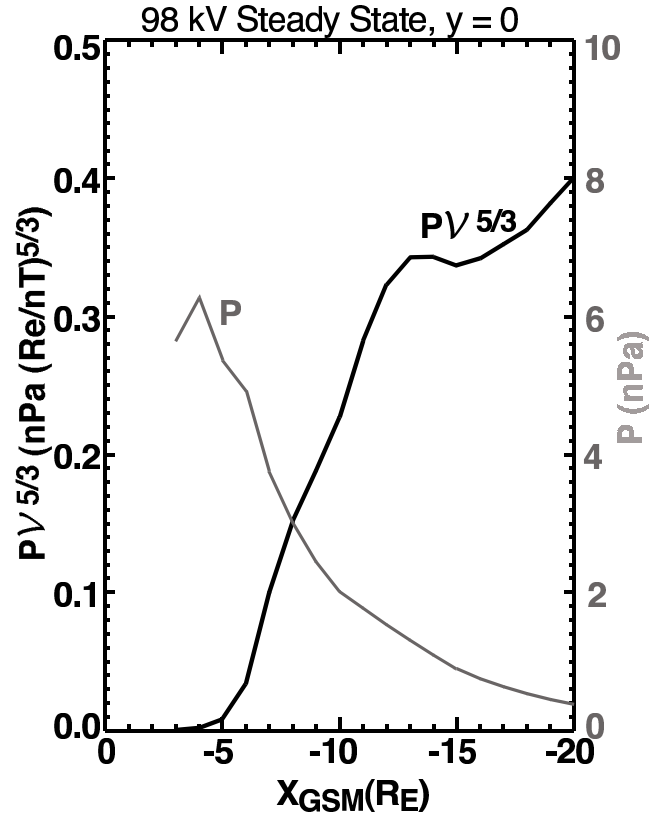


Fig. 4. Equatorial proton pressure and  $P\mathcal{V}^{5/3}$  at midnight MLT from the model of [22].

divergence in the heat flux vector [7], causing a reduction in entropy and thus  $P\mathcal{V}^{5/3}$  along drift paths. This reduction is seen in the model results of [21, 22] where the energy-dependent particle drift is included, as shown in Fig. 4 at the equator along the midnight meridian. The pressure balance inconsistency is based on conservation of  $P\mathcal{V}^{5/3}$  as particles electric field drift earthward on the nightside, whereas the model results show that the energy dependent magnetic drift cause  $P\mathcal{V}^{5/3}$  to decrease substantially along the midnight meridian. This gives plasma pressures at geosynchronous orbit, for example, that are more than a factor of four lower than would be if  $P\mathcal{V}^{5/3}$  were conserved along the midnight meridian.

#### 5. IMF and $P_{dyn}$ and Substorms

A reduction in the source term relative to the loss term in (1) will lead to a loss rate that exceeds the source rate and give  $(\partial/\partial t)(n\mathcal{V}) < 0$ . This will lead to a reduction in  $n\mathcal{V}$ ,  $P$ , and cross tail current as is necessary for current wedge formation and the onset of the expansion phase of substorms. This process is discussed in [15] and [13], where it is also addressed how this substorm process leads to a non-linear enhancement in the rate of current wedge formation and thus to the rapid development of the substorm expansion phase. The source term in (1) is proportional to  $\mathbf{V}_E$ , which equals  $E/B_e$ , where  $E$  is the electric field within the equatorial plasma sheet. On the other hand the loss term in (1) is proportional to  $P\mathcal{V}/B_e$ , which

varies as  $B_e^0$  to  $B_e^{-1/3}$  [15], and is thus nearly independent of  $E$  and  $B_e$ . Therefore a significant reduction in  $\mathbf{V}_E$  within the plasma sheet should lead to substorm onset, which can occur from a decrease in  $E$  or an increase in  $B_e$ . IMF changes modify  $E$ , and the magnetopause current changes resulting from  $P_{dyn}$  changes modify  $B_e$ , thus offering a plausible explanation for why substorm onset can be caused by either an IMF change that reduces  $E$  or a  $P_{dyn}$  increase. Note that the same particle divergence gives rise to both the Harang reversal during the substorm growth phase and the reduction in  $n\mathcal{V}$  when the strength of convection is reduced. Thus, following a reduction in convection, the maximum rates of reduction of  $n\mathcal{V}$  should occur within the region of the equatorial mapping of the Harang reversal, explaining why substorm onset is observed within the Harang region.

Typical increases in  $B$  on the nightside in responses to increases in  $P_{dyn}$  are  $\sim 10$  nT at synchronous orbit (e.g., [9]). Such an increase most often is not significant compared to  $B_e$  in the inner plasma sheet (which, from the Earth's dipole field alone, is  $\sim 100$  nT at geosynchronous orbit). However, modeling has shown that  $B_e$  can become below 10 nT within the  $r \sim 7-10 R_E$  region of the inner plasma sheet following prolonged periods of enhanced convection [20, 22], and  $B_e$  values below 10 nT have been observed within this region of the plasma sheet prior to substorm onset [11, 14]. Thus, an increase in  $P_{dyn}$  can cause a significant increase in  $B_e$  if it occurs following a period of strongly southward IMF, when  $B_e$  is substantially reduced within the inner plasma sheet. However, it is unlikely to do so under other situations. This is particularly important because increases in  $P_{dyn}$  have been observed to cause an increase in the strength of convection [2, 12], so that a large relative increase in  $B_e$  is necessary for an increase in  $P_{dyn}$  to reduce  $E/B_e$  and thus cause current wedge formation.

## 6. Null Events and Pseudo-Substorms

The above arguments also offer an explanation for the null events, since it is a decrease in  $\mathbf{V}_E$  that leads to current wedge formation. An IMF change leading to a reduction in  $E$  (such as a northward turning) that occurs simultaneously with a decrease in  $P_{dyn}$  can cause a simultaneous decrease in  $E$  and  $B_e$ , which could leave  $\mathbf{V}_E$  unchanged or increased within the inner plasma sheet. Similarly, an increase in  $P_{dyn}$  and a simultaneous IMF change that leads to an increase in  $E$  (such as a further southward turning) could leave  $\mathbf{V}_E$  unchanged or increased. In both cases, there would not be a decrease in  $\mathbf{V}_E$ , so that current wedge formation would not be expected to occur.

This nullification phenomenon also suggests a plausible explanation for pseudo-substorms where substorms initiate in a manner that is indistinguishable from a full substorm, but the expansion phase is terminated before full development (which is often defined as before expansion-phase auroral activity expands poleward to the polar-cap boundary). If an IMF or  $P_{dyn}$  trigger occurs and is soon followed (in  $\lesssim 10$  min) by an IMF or  $P_{dyn}$  change in the other direction (a nullifying change), then at first the source term in (1) would be reduced and substorm onset would proceed as it does following any other trigger. But then the source term would be increased, thus terminating the loss of particles necessary for further current wedge develop-

ment and thus ending the expansion phase development. Examples where this appears to have occurred are shown by [17].

## 7. Conclusions

We thus conclude that the physics of the particle transport that leads to the Harang electric field reversal offers a potential explanation for the IMF and  $P_{dyn}$  changes that do and do not cause substorm onset, as well as for SMCs and pseudo-storms as follows:

**SMCs:** The finite tail width together with the energy dependent magnetic drift gives particle & energy flux divergence that prevents excess build up of pressures. This allows for a stable balance within the inner plasma sheet between the source from inward convection and the loss from azimuthal magnetic drift.

**IMF & strong south IMF  $P_{dyn}$  substorms:** An IMF change or increase in  $P_{dyn}$  decreases the inner plasma sheet source from inward convection. It is necessary for  $B_e$  to be considerably lower than average for a  $P_{dyn}$  increase to trigger a substorm, so that such triggering only occurs after a period of strongly southward IMF.

**Null events:** Competing effects of an IMF or  $P_{dyn}$  trigger and a simultaneous nullifying IMF or  $P_{dyn}$  change lead to an approximately unchanged or increased source term.

**Pseudo-substorms:** A nullifying IMF or  $P_{dyn}$  change enhances the inner plasma sheet source term after onset, terminating substorm development before it becomes fully developed.

## Acknowledgements

This research was supported in part at UCLA by NSF grant OPP-0136139 and NASA grant NNG05GF29G. The work at Chungbuk National University was supported by the Korea Research Foundation grant funded by the Korean Government (MOEHRD) (KRF-2005-041-C00207).

## References

1. Baumjohann, W., R. J. Pellinen, H. J. Opgenoorth, and E. Nielsen, Joint two-dimensional observations of ground magnetic and ionospheric electric fields associated with auroral zone currents: Current systems associated with local auroral break-ups, *Planetary and Space Science*, 29, 431-447, 1981.
2. Boudouridis, A., E. Zesta, L. R. Lyons, P. C. Anderson, and D. Lummerzheim, Magnetospheric reconnection driven by solar wind pressure fronts, *Annales Geophysicae*, 22, 1367-1378, 2004.
3. Bristow, W. A., A. Otto and D. Lummerzheim, Substorm convection patterns observed by the Super Dual Auroral Radar Network, *Journal of Geophysical Research*, 106, 24,593-24,609, 2001.
4. Erickson, G. M., and R. A. Wolf, Is steady state convection possible in the Earth's magnetosphere?, *Geophysical Research Letters*, 6, 897, 1980.

5. Erickson, G. M., R. W. Spiro, and R. A. Wolf, The physics of the Harang discontinuity, *Journal of Geophysical Research*, *96*, 1633, 1991.
6. Gjerloev, J. W., R. A. Hoffman, E. Tanskanen, M. Friel, L. A. Frank, and J. B. Sigwarth, Auroral electrojet configuration during substorm growth phase, *Geophysical Research Letters*, *30*(18), 1927, doi: 10.1029/2003GL017851, 2003.
7. Heinemann, M., Role of collisionless heat flux in magnetospheric convection, *Journal of Geophysical Research*, *104*, 28,397–28,410, 1999.
8. Hughes, J. M., and W. A. Bristow, SuperDARN observations of the Harang discontinuity during steady magnetospheric convection, *Journal of Geophysical Research*, *108*(A5), 1185, doi:10.1029/2002JA009681, 2003.
9. Lee, D.-Y., and L. R. Lyons, Geosynchronous magnetic field response to solar wind dynamic pressure pulse, *Journal of Geophysical Research*, *109*, A04201, doi: 10.1029/2003JA010076, 2004.
10. Lee D.-Y., L. R. Lyons, G. D. Reeves, Comparison of geosynchronous energetic particle flux responses to solar wind dynamic pressure enhancements and substorms, *Journal of Geophysical Research*, *110*, A09213, doi:10.1029/2005JA011091, 2005.
11. Lui, A. T. Y. et al., A case study of magnetotail current disruption and diversion, *Geophysical Research Letters*, *15*, 721, 1988.
12. Lukianova R., Magnetospheric response to sudden changes in solar wind dynamic pressure inferred from polar cap index, *Journal of Geophysical Research*, *108*(A12), 1428, doi:10.1029/2002JA009790, 2003.
13. Lyons, L. R., and C.-P. Wang, Fundamental aspects of substorm onset, in *Substorms-7: Proceedings of the Seventh International Conference on Substorms*, p. 186, Finish Meteorological Institute, Finland, 2004.
14. Lyons, L. R., C.-P. Wang, T. Nagai, T. Mukai, Y. Saito, and J. C. Samson, Substorm inner plasma sheet particle reduction, *Journal of Geophysical Research*, *108*(A12), 1426, doi: 10.1029/2003JA010177, 2003a.
15. Lyons, L. R., C.-P. Wang, and T. Nagai, Substorm onset by plasma sheet divergence, *Journal of Geophysical Research*, *108*(A12), 1427, doi:10.1029/2003JA010178, 2003b.
16. Lyons, L. R., D.-Y. Lee, C.-P. Wang, and S. B. Mende, Global auroral responses to abrupt solar wind changes: Dynamic pressure, substorm, and null events, *Journal of Geophysical Research*, *110*, A08208, doi:10.1029/2005JA011089, 2005.
17. Lyons, L. R., D.-Y. Lee, S. Zou, C.-P. Wang, J. Weygand and S. B. Mende, External triggering and the large-scale nature of sawtooth event injections, *Journal of Geophysical Research*, submitted, 2006.
18. Nielson, E., Ionosphere-magnetosphere mapping of dynamic auroral structures during substorms, in *Auroral Physics*, p. 409, eds. C.-I. Meng, M. J. Rycroft, Cambridge University Press, Cambridge, UK, 1991.
19. Nielsen, E., and R. A. Greenwald, Variations in ionospheric currents and electric fields in association with absorption spikes during the substorm expansion phase, *Journal of Geophysical Research*, *83*, 5645, 1978.
20. Sergeev, V. A., T. I. Pulkkinen, R. J. Pellinen, and N. A. Tsyganenko, Hybrid state of the tail magnetic configuration during steady convection events, *Journal of Geophysical Research*, *99*, 23,571–23,582, 1994.
21. Wang, C.-P., L. R. Lyons, M. W. Chen, R. A. Wolf, and F. R. Toffoletto, Modeling the inner plasma sheet protons and magnetic field under enhanced convection, *Journal of Geophysical Research*, *108*, 10.1029/2001JA009620, 2003.
22. Wang, C.-P., L. R. Lyons, M. W. Chen, and F. R. Toffoletto, Modeling the transition of the inner plasma sheet from weak to enhanced convection, *Journal of Geophysical Research*, *109*, A12202, doi:10.1029/2004JA010591, 2004.
23. Weimer, D. R., D. M. Ober, N. C. Maynard, M. R. Collier, D. J. McComas, N. F. Ness, C. W. Smith, and J. Watermann, Predicting interplanetary magnetic field (IMF) propagation delay times using the minimum variance technique, *Journal of Geophysical Research*, *108*, 10.1029/2002JA009405, 2003.